

# $\pi\pi$ , $K\pi$ and $\pi N$ potential scattering and a prediction of a narrow $\sigma$ meson resonance

M. Sander and H.V. von Geramb\*

*Theoretische Kernphysik, Universität Hamburg, D-22761 Hamburg, Germany*

(October 26, 2018)

## Abstract

Low energy scattering and bound state properties of the  $\pi N$ ,  $\pi\pi$  and  $K\pi$  systems are studied as coupled channel problems using inversion potentials of phase shift data. In a first step we apply the potential model to explain recent measurements of pionic hydrogen shift and width. Secondly, predictions of the model for ponium lifetime and shift confirm a well known and widely used effective range expression. Thirdly, as extension of this confirmation, we predict an unexpected medium effect of the ponium lifetime which shortens by several orders of magnitude. The  $\sigma$  meson shows a narrow resonance structure as a function of the medium modified mass with the implication of being essentially energy independent. Similarly, we see this medium resonance effect realized for the  $K\pi$  system. To support our findings we present also results for the  $\rho$  meson and the  $\Delta(1232)$  resonance.

Typeset using REVTeX

---

\*e-mail: [hvg@i04ktha.desy.de](mailto:hvg@i04ktha.desy.de)

## I. INTRODUCTION

It is difficult to name hadronic systems for which the underlying QCD structure is manifest in low and medium energy observables [1]. The reason for this are the significantly different masses of nucleons and mesons as compared to the quark masses. As a consequence we may observe the QCD effects at very short interhadronic distances with an energy scale for excitations in the GeV and not as it is customary for nuclear physics in the MeV region. In the language of quantum mechanical radial wave functions we anticipate a situation similar to atomic physics where it is difficult to disclose effects of the nuclear realm. The interplay between low energy nuclear physics and QCD is tough since the phenomena are still difficult to identify and to associate with a particular substructure. Triggered by the need of a scalar isoscalar medium weight  $\sigma$  meson to understand the medium range nucleon–nucleon (NN) attraction, there exist many attempts to localize a resonance in  $L = 0, T = 0$   $\pi\pi$  scattering with a mass  $m_\sigma \sim 300 - 700$  MeV [2,3]. Despite all attempts, experimental data do not support the anticipated narrow resonance and theory gets acquainted with this situation.

We have been triggered by the development of a one solitary boson exchange model (OSBEP) [4] for NN scattering to study the  $\pi\pi$  and  $\pi$ –nucleon ( $\pi N$ ) system in terms of a potential model. The purpose of this investigation is to find a quantitative first guess for a dynamical model to describe the resonant particles  $\rho$ ,  $\sigma$ ,  $\Delta$  etc. It is intended to treat them explicitly as interacting multi pion and nucleon systems in an NN interaction model above meson production threshold. Undoubtedly, such a model is a subtle many–body problem for supercomputing.

Despite this motivation, there exists considerable interest in studies of di–hadronic systems which form Coulomb bound states [5,6]. Precision measurements of shifts and widths of such hydrogen like two body systems are supposed to sense with high accuracy the strong interaction at low energy. The shift is mainly caused by a modification at short distances where both the Coulomb and hadronic interactions are present while the width results from decay into energetically open channels. The decay can lead to a lower lying state of the same

system or into reaction channels. Candidates for such studies are all oppositely charged hadron pairs. From this sample, we selected pionic hydrogen ( $A_{\pi p}$ ) as a bound  $\pi^-$ -proton system and pionium ( $A_{\pi\pi}$ ) as a bound  $\pi^-\pi^+$  system both in relative s-states.

To describe such atomic systems it requires to know the hadronic interaction a priori or make a fit with a potential ansatz. The hadronic interaction is known, in the sense that the partial wave phase shifts are sufficient to determine the interaction by quantum inversion. This mathematical method uses spectral theory to transform the boundary conditions in form of the S-matrix or Jost function into a local energy independent potential [7]. The radial Schrödinger and Klein-Gordon equations are equivalent to a Sturm-Liouville problem on the half axis which is central for Gelfand-Levitan-Marchenko inversion. In Sec. II we show the salient features of inversion and give in Sec. III the potential results for  $\pi N$ ,  $\pi\pi$  and  $K\pi$  scattering. With these potentials all ingredients are specified for the treatment of  $A_{\pi p}$  and  $A_{\pi\pi}$  as coupled channel problems and predictions are given in Sec. IV. These predictions are in good agreement with experiment and lent support to our potential model.

As extension of the coupled channel potential model we treat  $\pi N$ ,  $\pi\pi$  and  $K\pi$  scattering in the continuum. The coupled equations, with Coulomb effects included, confirm that isospin is hardly broken and that resonance properties of all systems are quantitatively well described.

The p-wave resonances  $\Delta$  and  $\rho$  are contained in Secs. III.B and D respectively. S-wave channels of  $\pi\pi$  and  $K\pi$  scattering are treated in Sec. V. We attempt to solve the puzzle why a resonance is not visible in the phase shifts but at the same time meson exchange models require a medium weight  $\sigma$  meson with definitive particle properties. The solution to this investigation is a medium modification of the two body scattering which is manifest only in the  $T = 0$   $\pi\pi$  channel and  $T = 1/2$   $K\pi$  channel. The medium modification is identified with an effective mass in the coupled equations leading to a resonance structure as a function of effective mass and not of energy. Thus we observe a  $\sigma$  resonance width  $\Gamma \approx 1$  MeV practically independent of energy. Associated with this  $\sigma$  resonance is a shortening of lifetime of pionium  $A_{\pi\pi}$  by more than three orders of magnitude. The conclusions in Sec.

VI comprise the prediction of a very short range attraction close to the origin and a narrow high repulsive barrier at a relative distance  $r \approx 0.2$  fm for the  $\Delta$ ,  $\rho$ ,  $\sigma$  and  $K_0^*$  resonances. Comparable short range repulsions are seen for other channels. A confirmation of the long range interaction in terms of meson exchange is given and most importantly a narrow  $\sigma$  meson is predicted as a medium effect.

## II. POTENTIALS FROM INVERSION

Contrary to the direct path to obtain a potential for elementary particle scattering from QCD or other microscopic models we apply quantum inversion to experimentally determined phase shift functions as input in Gelfand–Levitan–Marchenko equations [7]. Nowadays, the inversion techniques for nucleon–nucleon scattering have evolved up to almost perfection for scattering data below pion production threshold. Numerically, input phase shifts can be reproduced for single and coupled channels with a precision of 1/100 of a degree, which is much lower than the experimental uncertainty. This accuracy and the possibility to test the inversion potential online, i. e. inserting the potential into the scattering equation and reproducing the input phase shifts, makes them a reliable and easy–to–handle tool for quantitative medium energy nuclear physics. Guided by this spirit, the utmost aim of quantum inversion is to provide a simple but accurate operator to reproduce data. This paradigm, however, proscribes to include sophisticated momentum dependencies or non–localities in the potential since this requires more information than can be extracted from phase shifts in a very limited energy domain. Our studies and applications are limited to the real phase shift domain but, for mathematical reasons, they are with smooth real functions extrapolated towards higher energies and infinity. This extrapolation is a kind of regularization which does not introduce spurious low energy phenomena and thus has no effect upon results and conclusions. This aspect of inversion has been investigated in important circumstances and we assume to be on save ground also in the applications studied hereafter. Furthermore, we are facing only single channel situations without Coulomb effects.

The basic equation of inversion is the Sturm–Liouville equation [8]

$$\left[ -\frac{d^2}{dx^2} + q(x) \right] y(x) = \lambda y(x). \quad (1)$$

We use the equivalent radial Schrödinger equation

$$\left[ -\frac{d^2}{dr^2} + \frac{\ell(\ell+1)}{r^2} + \frac{2\mu c^2}{(\hbar c)^2} V_\ell(r) \right] \psi_\ell(k, r) = k^2 \psi_\ell(k, r), \quad 0 \leq r < \infty \quad (2)$$

where  $V_\ell(r)$  is a local,  $k$ -independent operator in coordinate space and the factor  $2\mu c^2/(\hbar c)^2$  guarantees the correct units. Boundary conditions for the physical solutions are

$$\lim_{r \rightarrow 0} \psi_\ell(k, r) = 0 \quad (3)$$

and

$$\lim_{r \rightarrow \infty} \psi_\ell(k, r) = \exp(i\delta_\ell(k)) \sin\left(kr - \frac{\ell\pi}{2} + \delta_\ell(k)\right) \quad (4)$$

The Marchenko and the Gelfand–Levitan inversion are two inversion algorithm for the Sturm–Liouville equation which are briefly sketched for single channels and the case without a Coulomb reference potential. More details can be found elsewhere [7,9].

### A. Marchenko Inversion

The experimental information enters in the Marchenko inversion via the  $S$ -matrix, which is related to the scattering phase shifts by the relation

$$S_\ell(k) = \exp(2i\delta_\ell(k)). \quad (5)$$

We use a rational function interpolation and extrapolation of real data  $\delta_\ell(k)$ ,

$$\delta_\ell(k) = \sum_{m=1}^M \frac{D_m}{k - d_m} \quad (6)$$

with the boundary conditions

$$\lim_{k \rightarrow 0} \delta_\ell(k) \sim k^{2\ell+1} \quad \text{and} \quad \lim_{k \rightarrow \infty} \delta_\ell(k) \sim k^{-1}. \quad (7)$$

In any case there are 2–4 poles  $d_m$  and strengths  $D_m$  sufficient to provide a smooth description of data. Using a [4/4] or [6/6] Padé approximation for the exponential function  $e^z$  and substituting the rational phase function (6) into  $z = 2i\delta_\ell(k)$  gives a rational S–matrix

$$S_\ell(k) = 1 + \sum_{n=1}^{2N} \frac{s_n}{k - \sigma_n} = \prod_{n=1}^N \frac{k + \sigma_n^\uparrow}{k - \sigma_n^\uparrow} \cdot \frac{k + \sigma_n^\downarrow}{k - \sigma_n^\downarrow}, \quad (8)$$

using the notation  $\{\sigma_n^\uparrow\} := \{\sigma_n | \text{Im}(\sigma_n) > 0\}$  and  $\{\sigma_n^\downarrow\} := \{\sigma_n | \text{Im}(\sigma_n) < 0\}$ .

The Marchenko input kernel

$$F_\ell(r, t) = -\frac{1}{2\pi} \int_{-\infty}^{+\infty} h_\ell^+(kr) [S_\ell(k) - 1] h_\ell^+(kt) dk \quad (9)$$

is readily computed with the Riccati–Hankel functions  $h_\ell^+(x)$  and contour integration. This implies an algebraic equation for the translation kernel  $A_\ell(r, t)$  of the Marchenko equation

$$A_\ell(r, t) + F_\ell(r, t) + \int_r^\infty A_\ell(r, s) F_\ell(s, t) ds = 0. \quad (10)$$

The potential is obtained from the translation kernel derivative

$$V_\ell(r) = -2 \frac{d}{dr} A_\ell(r, r). \quad (11)$$

The rational representation of the scattering data leads to an algebraic form of the potential [7].

## B. Gelfand–Levitan Inversion

Gelfand–Levitan inversion uses Jost functions as input. The latter is related to the S–matrix by

$$S_\ell(k) = \frac{F_\ell(-k)}{F_\ell(k)}. \quad (12)$$

Using the representation (8), the Jost function in rational representation is given by

$$F_\ell(k) = \prod_{n=1}^N \frac{k - \sigma_n^\downarrow}{k + \sigma_n^\uparrow} = 1 + \sum_{n=1}^N \frac{B_n}{k + \sigma_n^\uparrow}, \quad (13)$$

or

$$|F_\ell(k)|^{-2} = 1 + \sum_{n=1}^N \frac{L_n}{k^2 - \sigma_n^2}. \quad (14)$$

The input kernel

$$G_\ell(r, t) = \frac{2}{\pi} \int_0^\infty j_\ell(kr) \left[ \frac{1}{|F_\ell(k)|^2} - 1 \right] j_\ell(kt) dk, \quad (15)$$

$j_\ell(x)$  the Riccati–Bessel functions, is analytic. The Gelfand–Levitan equation

$$K_\ell(r, t) + G_\ell(r, t) + \int_0^r K_\ell(r, s) G_\ell(s, t) ds = 0, \quad (16)$$

relates input and translation kernels and the potential is defined by

$$V_\ell(r) = 2 \frac{d}{dr} K_\ell(r, r). \quad (17)$$

For this potential an algebraic form is known [7].

Gelfand–Levitan and Marchenko inversions yield the same potential. Numerical instabilities can make the potentials differ but this signals in practice a problem and thus is permanently checked.

### III. INVERSION POTENTIAL RESULTS

Today, partial wave phase shift analyses are available for many hadronic systems. The best known of this sample is the NN analysis of Arndt *et al.* (SAID) which covers an energy range 0–1.3 GeV for  $np$  and 0–1.6 GeV for  $pp$  scattering [10]. The  $pp$  data are presently extended up to 3 GeV with measurements from the EDDA Collaboration of COSY in Jülich [11]. Of a similar quality is the  $\pi N$  analyses which is also available from SAID. Partial wave phase shifts of the  $\pi N$  system are determined by an analysis of elastic  $\pi^+p \rightarrow \pi^+p$ ,  $\pi^-p \rightarrow \pi^-p$  and charge exchange  $\pi^-p \rightarrow \pi^0n$  scattering. We use the solution SM95 of Arndt *et al.* [12]. This and all other analyses suppress Coulomb effects and assume good isospin. This implies that mass differences between  $\pi^\pm$  and  $\pi^0$  as well as proton and neutron are neglected. As a rule, for the pion is used  $m_\pi = m_{\pi^\pm} = 139.5676$  MeV and for the nucleon  $m_N = m_p = 938.27231$  MeV respectively. Included is also the Karlsruhe–Helsinki analysis

of Koch and Pietarinen KH80 [13]. For  $\pi\pi$  scattering we use phase shifts from the analysis of Frogatt and Petersen [14] and theoretical predictions from a meson exchange potential by Lohse *et al.* [15] and chiral perturbation theory by Gasser and Leutwyler [16]. Finally, the  $K\pi$  analysis of Estabrooks *et al.* uses final state interactions of  $K^\pm p \rightarrow K^\pm \pi^+ n$  and  $K^\pm p \rightarrow K^\pm \pi^- \Delta^{++}$  [17]. We restrict our analyses herein to  $L = 0$  and 1 partial waves with isospins  $T = 1/2$  and  $3/2$  for  $\pi N$  and  $K\pi$ , and  $T = 0,1$  and 2 for the  $\pi\pi$  systems. A comprehensive analysis of data and inversion potentials can be found elsewhere [9]. We are using the elastic domain phase shifts and thus limit the input to  $T_{lab} < 500$  MeV for  $\pi N$ ,  $M_{\pi\pi} < 970$  MeV and  $M_{K\pi} < 1.3$  GeV. Resonance effects, like the  $f_0(975)$  in  $\pi\pi$  scattering, are not included.

### A. $\pi N$ s-wave scattering

The notation of this channel distinguishes  $S_{11}$  and  $S_{31}$  partial waves to signal angular momentum  $L = 0$ , isospins  $T = 1/2$  and  $3/2$  and spin  $S = 1/2$  states. Input phase shifts from SM95 and KH80 are shown in Fig. 1 and the inversion potentials are given in Fig. 2 respectively. In Sec. IV.A these potentials are used to study pionic hydrogen.

As a brief note we mention the assessment of the pion nucleon coupling constant from these potentials. From the  $\pi N$  potentials in the  $T = 1/2, 3/2$  s-channels we find the scattering lengths  $a_1 = 0.178 m_\pi^{-1}$  and  $a_3 = -0.088 m_\pi^{-1}$ . For a comparison with several other predictions see Table I. These results may be used in the Goldberger–Miyazawa–Oehme sum rule [20]

$$\frac{f_{\pi NN}^2}{4\pi} = \frac{(m_\pi^2 - \mu^2)(m_N + m_\pi)}{6m_N m_\pi} (a_1 - a_3) - \frac{m_\pi^2 - \mu^2}{8\pi^2} \int_0^\infty \frac{\sigma_{\pi^- p} - \sigma_{\pi^+ p}}{\sqrt{q^2 + m_\pi^2}} dq \quad (18)$$

to obtain a model independent estimate for the  $\pi NN$  coupling constant. Using the simplified form of this sum rule

$$\frac{f_{\pi NN}^2}{4\pi} = 0.19 m_\pi (a_1 - a_3) - (0.025 \text{ mb}^{-1}) \mathcal{J}, \quad (19)$$

where the integral



$$\mathcal{J} = \frac{1}{4\pi^2} \int_0^\infty \frac{\sigma_{\pi^-p} - \sigma_{\pi^+p}}{\sqrt{q^2 + m_\pi^2}} dq \quad (20)$$

has the VPI value  $\mathcal{J} = -1.041$  mb. We find

$$\frac{f_{\pi NN}^2}{4\pi} = 0.0766, \quad \text{or} \quad \frac{g_{\pi NN}^2}{4\pi} = 13.84, \quad (21)$$

which is fully consistent with the value of  $13.75 \pm 0.15$  given in [12].

### B. $\pi N$ p-wave scattering

Most prominent is the  $\Delta(1232)$  or  $P_{33}$  resonance which we treat with great care. The low energy phase shift function, shown in Fig. 3, uses SM95 and KH80 data. A factorization of the S-matrix into a resonant and a non-resonant background part  $S(k) = S_r(k)S_b(k)$  is useful. For the resonant part a resonance and an auxiliary pole parameterization

$$S_r(k) = \frac{(k + k_r)(k - k_r^*)(k + k_h)(k - k_h^*)}{(k - k_r)(k + k_r^*)(k - k_h)(k + k_h^*)} \quad (22)$$

is used. It contains the right amount of zeros and poles for a decomposition into Jost functions. The background  $S_b(k)$  is smooth but its shape depends on the parameters in (22). Actual values are taken from data tables [21] for  $k_r$  and  $k_h = 0.5 + i10 \text{ fm}^{-1}$ . The inversion potential is independent from this splitting and is shown in Fig. 4. The resonance feature is generated from the short range attraction near the origin and is limited by a narrow (0.1 fm) potential barrier with a height of  $\sim 20$  GeV. Being accustomed to strengths and ranges of NN potentials it is surprising to see this small radial dimension and large potential strength. After a second thought this is not a surprise since inversion is a kind of generalized Fourier transformation and thus the units are a consequence of the pion mass and the quantitative behavior of the phase shift. Nevertheless, the potential changes occur at very small radii compared to the size of the charge form factors of pion and nucleon. The RMS radii are known to be 0.54 fm for the pion and 0.7 fm for the nucleon. Our radius describes the distance of the center of masses and  $r = 0.16$  fm, the barrier radius, implying more than 90% overlap of the intrinsic structures. We conjecture for the barrier a

simulation of a transition from the pion–nucleon quark content into the 3–quark content of the  $\Delta$ . Ultimately, such explanation must be confirmed by QCD calculations.

In Fig. 5 we illustrate the  $P_{33}$  potential resonance showing the physical solution  $|u(E, r)/r|^2$  as a function of energy and radius. This figure shows that the probability builds up between the origin and the barrier.

The long range part of the inversion potential, not visible in Fig. 4, behaves like a Yukawa tail with a strength  $Y = 650.0$  MeVfm and an effectively exchanged mass of 350 MeV. There exists no physical particle with this mass since in the meson exchange picture s– and t–channel graphs contribute.

### C. $\pi\pi$ s–wave scattering

$\pi\pi$  phase shifts come from the analysis of final state interactions in  $\pi N \rightarrow \pi\pi N$  systems or the  $K_{e4}$ –decay  $K^- \rightarrow \pi^+\pi^-e\bar{\nu}$ . Here we use results of the CERN–Munich experiment [14]. The scattering is purely elastic until  $M_{\pi\pi} = 987.3$  MeV where coupling to the  $K\bar{K}$  opens and the phase shift becomes highly inelastic and resonant in the  $T = 0$  channel. The  $T = 2$  channel remains smooth. A summary of all experimental phase shifts and theoretical predictions, from a meson exchange model [15] and chiral perturbation theory [16], is shown in Fig. 6. Notation for the isospin and angular momentum channels uses  $\delta_\ell^T$  or  $V_\ell^T$ . The three used phase shift sources yield slightly different inversion potentials, shown in Fig. 7. It is obvious that  $\pi\pi$  phase shifts are less well established than  $\pi N$  data. Table II comprises a summary of effective range parameters from different sources to substantiate the uncertainties.

### D. $\pi\pi$ p–wave scattering

As before, phase shifts come from the analysis of final state interactions in  $\pi N \rightarrow \pi\pi N$  systems. Isospin is limited to the single value  $T = 1$  and the CERN–Munich analysis is used [14]. The scattering is dominated by the  $\rho$  resonance,  $m_\rho = 770$  MeV,  $\Gamma = 150$  MeV, and

the phase shift remains essentially real until  $M_{\pi\pi} = 1.2$  GeV. The used phase shift is shown in Fig. 8 and the inversion potential is shown in Fig. 9. Notice the barrier maximum at 0.16 fm which is the same as seen in the  $\pi N P_{33}$  channel. We decline from repeating the resonance wave function display due to its similarity with results shown in Fig. 5.

### E. $K\pi$ s-wave scattering

Phase shifts are taken from the Estabrooks *et al.* analysis [17]. We distinguish between isospins  $T = 1/2$  and  $3/2$ . As shown in Figs. 10 and 11, this systems resembles the  $\pi\pi$  s-wave scattering. The long range part of the two isospin potentials are numerically very close outside  $r = 0.4$  fm which supports isospin independence. Furthermore, outside  $r = 0.8$  fm both potentials are very small,  $|V_0^{2T}(r)| < 1$  MeV. This weak medium and long range interaction requires further investigations but we notice the same feature for  $K^+N$  inversion potentials, consistent with the extraordinary long mean free path of kaons in nuclear matter [34,9]. We shall show that this system displays similar medium effects as the corresponding  $\pi\pi$  system.

## IV. COUPLED SYSTEMS

Pionic-hydrogen  $A_{\pi p}$  is treated in a coupled channel calculation as a charge exchange resonance seen in  $\pi^0$ -neutron scattering. There exists a spectrum of excited states with different relative angular momenta but only the s-states shall be studied for comparison with experiment. Similarly,  $A_{\pi\pi}$  is formed by  $\pi^-\pi^+$  and it is treated as a charge exchange resonance state seen in the elastic  $\pi^0\pi^0$  channel.

The coupled system is written in the form

$$f_i'' + k_i^2 f_i = \sum_{j=1}^2 \frac{2\mu_i}{\hbar^2} V_{ij} f_j, \quad (23)$$

and uses conventionally  $i = 1(2)$  as the reaction (elastic entrance) channel.

## A. Pionic hydrogen

The reduced masses enter in our calculation with two options. In the first case we use only the mass of the charged pion and the proton mass,  $\mu_1 = \mu_2$  with

$$\mu_1 = \frac{m_{\pi^-} m_p}{(m_{\pi^-} + m_p)}. \quad (24)$$

In the second case we use  $\mu_1 \neq \mu_2$  and use for  $\mu_2$  the physical masses of the neutral particles

$$\mu_2 = \frac{m_{\pi^0} m_n}{(m_{\pi^0} + m_n)}. \quad (25)$$

The potential matrix contains the Clebsch–Gordan coefficients for the rotation of the interaction from good isospin into particle states.

$$V_{11} = V^{\pi^- p} = \frac{1}{3}V_s^{3/2} + \frac{2}{3}V_s^{1/2} - \frac{e^2}{r}, \quad (26)$$

$$V_{12} = V_{21} = \frac{\sqrt{2}}{3}(V_s^{3/2} - V_s^{1/2}), \quad (27)$$

$$V_{22} = V^{\pi^0 n} = \frac{2}{3}V_s^{3/2} + \frac{1}{3}V_s^{1/2}. \quad (28)$$

The kinematics is expressed in any case by the physical masses and projectile kinetic energy  $T_{lab}$

$$S = (m_{\pi^0} + m_n)^2 + 2T_{lab}m_n \quad (29)$$

$$k_1^2 = \frac{S^2 + (m_{\pi^-}^2 - m_p^2)^2 - 2S(m_{\pi^-}^2 + m_p^2)}{4S(\hbar c)^2} \quad (30)$$

$$k_2^2 = \frac{m_n^2 T_{lab} (T_{lab} + 2m_{\pi^0})}{S(\hbar c)^2}, \quad (31)$$

which guarantees the correct threshold behavior.

The Coulomb attraction between  $\pi^-$  and  $p$  causes a bound system which is known as pionic hydrogen  $A_{\pi p}$ . In addition to Coulomb attraction, the hadronic interaction between the two constituents distorts the short range interaction and changes the pure Coulomb spectrum. Decay channels are  $\pi^- p \rightarrow \pi^0 n + 3.30023$  MeV and  $\pi^- p \rightarrow n\gamma$ . The hadronic shift of the  $3p \rightarrow 1s$  transition and the total  $1s$  width has been measured at PSI [5]. To analyze this experiment we use the described potential model. Inelasticities, Coulomb and

other isospin breaking effects are supposed to be not included in the SM95 phase shift analysis and the real potential matrix is shown in Fig. 12. We use the reduced masses  $\mu_1 = \mu_2 = 121.4970$  MeV which are consistent with the phase shift analysis and using  $\pi^\pm$  and  $p$  masses. Alternatively  $\mu_1 = 121.4970$  MeV and  $\mu_2 = 118.0216$  MeV based upon  $\pi^0$  and neutron masses respectively can be used.

The bound states of the  $\pi^-p$  system can be found as resonances in the energetically open  $\pi^0n$  channel. The width (FWHM) of this resonance accounts only for the decay of  $\pi^-p \rightarrow \pi^0n$ . Table III contains this result in the first line. To evaluate the hadronic shift we used in all cases the reference energy  $E_{1s}^C = 3234.9408$  eV. The shift is calculated as the difference between  $E_{1s}^C$  and the calculated resonance energy taken at the maximum of the elastic scattering cross section

$$\sigma(\pi^0n \rightarrow \pi^0n) = \frac{\pi}{k_2^2} |1 - S_{22}|^2. \quad (32)$$

From this distribution we obtain also the FWHM. The Coulomb potential is contained in  $V_{11}$  as determined from point charges  $V^C = e^2/r$  or double folded Gaussian charge distributions  $V^C = e^2\Phi(1.13r)/r$ .  $\Phi(r/\alpha)$  is the error function and  $\alpha = \sqrt{\langle r_\pi^2 \rangle + \langle r_p^2 \rangle}$  with RMS radii  $\langle r_\pi^2 \rangle^{1/2} = 0.5389$  fm and  $\langle r_p^2 \rangle^{1/2} = 0.702$  fm. To compare with experimental data [5] we evaluated the partial width  $\Gamma_{1s}^{\pi^0n}$  using the Panofsky ratio  $P = 1.546 \pm 0.009$  [35],

$$\Gamma = \left(1 + \frac{1}{P}\right) \Gamma^{\pi^-p \rightarrow \pi^0n}. \quad (33)$$

To account also for decay into the  $n\gamma$  channel from the  $\pi^0n$  channel an imaginary potential  $W_{11} = -9 \exp(-9r^2)$  MeV is added to  $V_{11}$  which brings the theoretical results in agreement with experiment. Other corrections are not further pursued since they enter into the reference and resonance energy with approximately the same amount, affecting the difference by  $< \pm 0.01$  eV. We shall not dwell upon this issue in more detail herein. The essential result of this part of our calculation is that isospin breaking effects due to mass differences are small.

## B. Pionium

Very close the same convention as for  $A_{\pi p}$  is used here. Only one value of a reduced mass occurs

$$\mu_1 = \mu_2 = \frac{m_{\pi^+}}{2}. \quad (34)$$

This value is varied in Sec. V.A when medium effects are discussed. The potential matrix is readily expressed by

$$V_{11} = V^{\pi^+\pi^-} = \frac{1}{3}V_0^2 + \frac{2}{3}V_0^0 - \frac{e^2}{r}, \quad (35)$$

$$V_{12} = V_{21} = \frac{\sqrt{2}}{3}(V_0^2 - V_0^0), \quad (36)$$

$$V_{22} = V^{\pi^0\pi^0} = \frac{2}{3}V_0^2 + \frac{1}{3}V_0^0, \quad (37)$$

and the kinematics by

$$S = 4m_{\pi^0}^2 + 2T_{lab}m_{\pi^0} \quad (38)$$

$$k_1^2 = \frac{S - 4m_{\pi^-}^2}{4(\hbar c)^2} \quad (39)$$

$$k_2^2 = \frac{m_{\pi^0}^2 T_{lab}(T_{lab} + 2m_{\pi^0})}{S(\hbar c)^2} \quad (40)$$

$$M_{\pi\pi} = \sqrt{S} \quad (41)$$

Similar to the  $A_{\pi p}$  system there exists pionium  $A_{\pi\pi}$  which is formed by  $\pi^-\pi^+$  Coulomb attraction. It decays predominantly by charge exchange into the open  $\pi^0\pi^0$  channel. The coupled channel system is defined with Eqn. (23). We assume the same approach as for  $A_{\pi p}$  and rotate the good isospin potentials into particle states. The hadronic potential matrix is shown in Fig. 13 using the three different sources discussed in Sect. III.C. Phase shift analyses and inversion use a single mass  $\mu_1 = \mu_2 = \mu = m_{\pi^+}/2$  without Coulomb effects. This assumption guarantees good isospins  $T = 0$  and 2. The results of our calculations are summarized in Table IV. A point Coulomb reference energy  $E_{1s}^C = 1.85807248$  keV is used. With this choice of masses and the correct Q-value our calculations agree practically with some well known scattering length expressions which is most often used [6,36,37]

$$\frac{1}{\tau} = \frac{8\pi}{9} \left( \frac{2\Delta m}{\mu} \right)^{\frac{1}{2}} \frac{(a_0^0 - a_0^2)^2 |\Psi(0)|^2}{1 + \frac{2}{9}\mu\Delta m (a_0^0 + 2a_0^2)^2} \quad (42)$$

$$\approx 1.43 (a_0^0 - a_0^2)^2 |\Psi(0)|^2, \quad (43)$$

where  $\Delta m$  is the mass difference  $m_{\pi^+} - m_{\pi^0}$ . The real interesting result of this study comes from dramatic changes (shortening) of the  $A_{\pi\pi}$  lifetime, by several orders of magnitude, with small variations of the reduced masses  $\mu_i$ .

## V. MEDIUM EFFECTS

Low energy nuclear physics associates medium effects with changes of the free interaction potential or free two body scattering amplitudes in the presence of a few- or many-body environment. Effective interactions incorporate such effects and degrades the environment into the role of spectators. A well known example is the nuclear matter g-matrix which includes Pauli blocking and selfconsistent mean field effects and which is related to the free two body t-matrix. Other medium modification are due to recoil, truncation of coupled channels and relativistic corrections to name a few. Medium effects from meson and boson exchange models are related to restoration mechanism of the broken chiral symmetry in nuclear matter. This field of research is presently in the center of different theoretical lines of thought and some of them are found in [38].

Our concern is an effective mass in the two particle wave equation which may have different causes in few and many body systems. At this stage the consequences and dynamical effects are shown for the two particle subsystems  $\pi\pi$  and  $K\pi$  in case an effective mass is assumed. What we study are partial wave phase shifts  $\delta(E, m)$  as a function of energy and the effective mass, which determines the reduced masses  $\mu_i$  in Eqn. (34). Effects upon the lifetime of pionium are also studied.

### A. $\pi\pi$ scattering

In Sect. IV.B results of pionium lifetime and hadronic shift are given. This study uses the  $\pi^\pm$  mass consistently with the phase shift analyses and the scattering length expressions for the life time. Here we extend this study and show results in Fig. 14 for the hadronic shift and lifetime of pionium as a function of the pion mass,  $m_\pi = 2\mu_1 = 2\mu_2$  in Eqs. (34). The potential matrix  $V_{ij}$  was unchanged and the  $k_i^2$  values computed with the physical masses of  $\pi^\pm$  and  $\pi^0$  as defined in Eqs. (38–41). With this prescription we effectively change the total strength of the potential matrix  $V_{ij}$  by  $\pm 1\%$  and observe a variation of the shift by two orders of magnitude and of the lifetime by three orders of magnitude. The physical mass result is accentuated. The interval of mass variation is small compared with the physical mass differences between  $\pi^\pm$  and  $\pi^0$  of 4.6 MeV, which a correct phase shift analysis should consider. Since this is not the case, consistency requires to use  $\mu_1 = \mu_2$  in the inversion procedure and in the coupled channel calculations. Thus, we maintain the assumption of a good isospin also for the calculation with an effective mass.

Triggered from this result we extended our calculations for the eigenchannel phase shifts of the coupled system which coincide with the uncoupled good isospin calculations for  $T = 0$  and 2. In Fig. 15 we show the  $L = 0$ ,  $T = 0$  phase shift  $\delta_0^0(m, T)$  as a function of the effective mass  $m = 2\mu_1 = 2\mu_2$  and the laboratory kinetic energy. The physical mass result is emphasized and follows the result shown in Fig. 6 for  $\delta_0^0$ . As a function of mass we observe a typical resonance behavior whose width  $\Gamma = 1 - 2$  MeV which is almost energy independent. The resonance feature is supported by Fig. 16 which shows  $|u(r, m, T)/r|^2$  as a function of radius and effective mass for three kinetic energies. Since  $L = 0$ , the radial wave function is  $\neq 0$  at the origin around which the probability is build up. This figure should be compared with Fig. 5 of the  $\pi N \Delta$  resonance which shows the same pattern as a function of energy. For the  $\pi N P_{33}$  phase shift  $\delta(E)$  varies only insignificantly when the reduced mass of pion–nucleon system is modified within 1 MeV and the resonance pole is stable against this variation. From the  $\pi N$  potential in Fig. 4 the same mass dependence



as for the  $\pi\pi$  system was expected. This is not the case. We attribute this stability to the boundary condition of the p-wave at the origin to be zero. The  $\pi\pi$  s-wave  $T = 0$  potential in Fig. 7 supports the resonance as function of mass since no boundary condition at the origin restricts the development of a large amplitude breathing mode. The potentials have in both cases a very high barrier of 20 – 30 GeV, compared to the kinetic energy of several 100 MeV, which is narrow  $\sim 0.1$  fm and within the barrier the potentials are very deep. For the s- and p-waves decays the radial wave exponentially practically independent from the projectile energy. However, the boundary condition of the p-wave at the origin suppresses the free unfolding of a resonance amplitude independent from energy. It requires an optimal matching of the external wave function to realize the internal resonance enhancement. A small variation of the potential depth within the barrier does not overcome the restriction from the boundary condition for the p-wave. This situation is essentially different for s-waves. For them it is important to have the correct wave number within the barrier that the wave function matches the exponentially decaying function in the barrier optimally. The wave number within the barrier is determined by

$$k^2 = \frac{(M_{\pi\pi} - (2\mu/m_{\pi^+})V(r))^2 - 4m_{\pi^+}^2}{4(\hbar c)^2}. \quad (44)$$

A small variation of the reduced mass  $\mu$  produces the discussed effect. In connection with the very high barrier gives this the explanation of the projectile independence of the observed  $\pi\pi$  resonance as a function of the effective mass. The high barrier decouples for s-waves the inner from the exterior dynamics which is not the case for p- and higher partial waves.

Finally, the effective mass used in this study must be the result of embedding the  $\pi\pi$  system into a few- and many-body environment. In the meson exchange models for NN scattering should the correlated two pion exchange dynamics not be determined from the physical free pion mass but from an effective mass. This mechanism is able to change the non-resonant two pion system into a resonant system with a width  $1 < \Gamma < 600$  MeV. The lower limit is extracted from Fig. 15 and the upper limit is deduced from the free system  $\delta_0^0(e)$  [2]. This gives a possible explanation of the properties of the  $\sigma$ -meson used in all high

quality meson exchange model for hadron–hadron interactions out of which the NN potentials are the best examples. The phase shift  $\delta_0^2(E, m)$  shows practically no mass dependence and maintains its repulsive nature.

To support this picture for  $\pi\pi$  scattering it is obvious to look for other systems with the same properties.

### B. $K\pi$ scattering

Phase shift data for the  $K\pi$   $s$ -wave scattering yield qualitatively the same situation with two possible isospin couplings  $T = 1/2$  and  $3/2$ . The inversion potentials are shown in Fig. 11. A purely repulsive potential is seen for the  $T = 3/2$  channel whereas  $T = 1/2$  has a narrow and high potential barrier at about the same radial region as the  $\pi\pi$  system and we expect great similarities with respect to the phase shifts  $\delta_0^1(m, T)$ , a functions of effective mass and kinetic energy. Fig. 17 confirms this conjecture. Following the same line for the coupled system in Sec. IV, one effective mass parameter is used  $m = 2\mu_{K\pi}$  where the physical mass has a value of 215.94 MeV. The solid line signals the physical  $T = 1/2$  phase shift and the energy–mass distribution shows a resonance structure. The width increases,  $\Gamma > 80$  MeV, with laboratory kinetic energy which is caused by the relative smallness of the barrier of 800 MeV. The phase shifts  $\delta_0^3(E, m)$  shows no mass dependence and maintains its repulsive nature.

## VI. SUMMARY

The elastic scattering domain for  $\pi\pi$ ,  $K\pi$  and  $\pi N$  scattering is investigated with the help of a local  $r$ -space potential model. Quantum inversion is used to generate from phase shift data the potentials for low partial waves and the permitted isospin channels. Tables of these potentials are available [39]. All resonance features visible in the phase shifts are well accounted for,  $\rho$  and  $\Delta$  are potential resonances of a  $\pi\pi$  and  $\pi N$  system respectively.

Pionic hydrogen  $A_{\pi p}$  is studied as a resonance in elastic  $\pi^0$ -neutron scattering below  $\pi^-$ -proton threshold. The calculated shift and width of the ground state agree very well with recent measurements. Similarly, ponium  $A_{\pi\pi}$  is studied as a resonance in elastic  $\pi^0\pi^0$  scattering below  $\pi^+\pi^-$  threshold. The potential model confirms well known scattering length expressions often used with hadronic bound state problems. As a new feature we disclose a medium effect of lifetime and shift of  $A_{\pi\pi}$  when the interaction strength is increased by typically half a percent. The amount of change is more than three orders of magnitude. In an extended study a medium resonance is identified with the  $\sigma$  resonance. In particular it is shown that this resonance is a function of the effective mass, which we identify as the factor in front of the potential, and not as it is common as a function of energy. It can be considered as a parametric resonance. The change of  $A_{\pi\pi}$  lifetime is a feature of this resonance. A similar situation with medium effects and a parametric resonance is identified in the  $K\pi$   $L = 0$ ,  $T = 1/2$  channel. Contrary to this medium resonances show the classic  $\rho$  and  $\Delta$  resonances practically no effective mass dependence. Showing radial wave functions we explain these differences of dynamical behavior with boundary conditions at the origin. All resonances are associated with a small radial region within 0.3 fm. This distance is the center of mass distance of the two particles and is not the QCD bag radius. Table V shows that the potential barriers which trap the relative system are very close the same with the exception of the strange  $K\pi$  resonance. In view of the large RMS radii of mesons and nucleons ( $\sim 0.6$  fm) this implies a more than 90 percent overlap of the individual QCD bags before fusion occurs and the new configuration develops. We see in this universal small barrier radius a reason why meson exchange works and permits quantitatively to describe NN and other hadron-hadron interactions. This finding requires detailed calculations on the QCD level.

For low and medium energy nuclear physics this potential model defines essential ingredients of boson exchange models in terms of  $\pi$  mesons and nucleons only.  $\rho$  and  $\Delta$  resonances are well accounted for their properties with the inversion potentials and the  $\sigma$  meson shows dynamic aspects which does not support it as a particle. Since long there exist experimental

data which involve two pion production and still lack of satisfactory explanation. It is known as ABC effect [40] and we suggest a re-analysis of this data with the discussed dynamical effects included. The set of inversion potentials can easily be completed [9] to have a basis for potential model calculations which use only pions, protons and neutrons. This opens the possibility for quantitative fragmentation calculations requiring massive supercomputing.

#### **ACKNOWLEDGMENT**

The authors appreciate the constructive discussions with R. Jahn, H. Markum, D. Bugg, L. Jäde and G. Steinbach. This work was supported in part by Forschungszentrum Jülich GmbH under Grant-Nr. 41126865.

## REFERENCES

- [1] T. Barnes, E.S. Swanson and J. Weinstein, Phys. Rev. **D46**, 4868 (1992); T. Barnes, S. Capstick, M.D. Kovarik and E.S. Swanson, Phys. Rev. **C48**, 539 (1993); J. Weinstein, *The multichannel quark model*, LANL e-print archive nucl-th/9606037
- [2] M. Harada, F. Sannino and J. Schechter, Phys. Rev. **D54**, 1991 (1996)
- [3] N.A. Törnqvist and M. Roos, Phys. Rev. Lett. **76**, 1575 (1996); N. Isgur and J. Speth, *ibid.* **77**, 2332 (1996); N.A. Törnqvist and M. Roos, *ibid.* **77**, 2333 (1996)
- [4] L. Jäde and H.V. von Geramb, Phys. Rev. **C55**, 57 (1997)
- [5] D. Sigg et al., Phys. Rev. Lett. **75**, 3245 (1995)
- [6] L.G. Afanasyev et al., Phys. Lett. **B338**, 478 (1994)
- [7] K. Chadan and P.C. Sabatier, *Inverse Problems in Quantum Scattering Theory, 2nd. Edition*, Springer, Berlin (1989); H.V. von Geramb (ed.), *Quantum Inversion Theory and Applications*, Lecture Notes in Physics 427, Springer (1994)
- [8] B.M. Levitan, *Inverse Sturm–Liouville Problems*, VNU Science Press, Utrecht (1987)
- [9] M. Sander, *Quanteninversion und Hadron–Hadron Wechselwirkungen*, ISBN 3–8265–2129–3, Shaker Verlag (1997)
- [10] R.A. Arndt et al., Phys. Rev. **C50**, 2731 (1994)
- [11] D. Albers et al., Phys. Rev. Lett. **78**, 1652 (1997)
- [12] R.A. Arndt, I.I. Strakowsky, R.L. Workman and M.M. Pavan, Phys. Rev. **C52**, 2120 (1995)
- [13] R. Koch and E. Pietarinen, Nucl. Phys. **A336**, 331 (1980)
- [14] C.D. Froggatt and J.L. Petersen, Nucl. Phys. **B129**, 89 (1977)
- [15] D. Lohse, J.W. Durso, K. Holinde and J. Speth, Nucl. Phys. **A516**, 513 (1990)

- [16] J. Gasser and H. Leutwyler, Phys. Lett. **125B**, 325 (1983); Ann. Phys. (N.Y.) **158**, 142 (1984)
- [17] P. Estabrooks et al., Nucl. Phys. **B133**, 490 (1978)
- [18] B.C. Pearce and B.K. Jennings, Nucl. Phys. **A528**, 655 (1991)
- [19] C. Schütz, J.W. Durso, K. Holinde and J. Speth, Phys. Rev. **C49**, 2671 (1994)
- [20] R.L. Workman, R.A. Arndt and M.M. Pavan, Phys. Rev. Lett. **68**, 1653 (1992)
- [21] Particle Data Group, Phys. Rev. **D54**, 1 (1996)
- [22] P. Estabrooks and A.D. Martin, Nucl. Phys. **B79**, 301 (1974)
- [23] G. Grayer et al., Nucl. Phys. **B75**, 189 (1974)
- [24] W. Männer, Contribution to the IVth Int. Conference on Experimental Meson Spectroscopy, Boston, Mass. (1974)
- [25] P. Baillon et al., Phys. Lett. **38B**, 555 (1972)
- [26] S. Weinberg, Phys. Rev. Lett. **17**, 616 (1966); *ibid.* **18**, 188 (1967)
- [27] L. Rosselet et al., Phys. Rev. **D15**, 574 (1977); M.M. Nagels et al., Nucl. Phys. **B147**, 189 (1979)
- [28] E.A. Alekseeva et al., Sov. Phys. JETP **55**, 591 (1982)
- [29] H. Burkhardt and J. Lowe, Phys. Rev. Lett. **67**, 2622 (1991); D. Počanić et al., Phys. Rev. Lett. **72**, 1156 (1994)
- [30] M.G. Olson, *Rigorous pion-pion scattering lengths from threshold  $\pi N \rightarrow \pi\pi N$  data*, Preprint MADPH-97-988, LANL e-print archive hep-ph/9703247
- [31] W. Ochs,  $\pi N$  Newsletter **3**, 25 (1991)
- [32] S.D. Protopopescu et al., Phys. Rev. **D 7**, 1279 (1973)

- [33] B.B. Deo and J.K. Mohapatra, *Pramana* **18**, 39 (1982)
- [34] C.B. Dover and G.E. Walker, *Phys. Rep.* **89**, 1 (1982)
- [35] J. Spuller et al., *Phys. Lett.* **B67**, 479 (1977)
- [36] G.V. Efimov, M.A. Ivanov and V.E. Lyubovitskii, *Sov. J. Nucl. Phys.* **44**, 296 (1986)
- [37] J.L. Uretsky and T.R. Palfrey, Jr., *Phys. Rev.* **121**, 1798 (1961)
- [38] R. Rapp, J.W. Durso and J. Wambach, Preprint SUNY-NTG-96-42
- [39] Use the URL <http://i04ktha.desy.de>
- [40] A. Abashian, N. E. Booth and K. M. Crowe, *Phys. Rev. Lett.* **5**, 258 (1960); *ibid.* **7**, 35 (1961);

TABLES

TABLE I.  $\pi N$   $s$ -wave scattering lengths and  $\pi NN$  coupling constant obtained from the GMO sum rule.

Model	$a_1 [m_\pi^{-1}]$	$a_3 [m_\pi^{-1}]$	$f_{\pi NN}^2/4\pi$	Ref.
SM95 Inversion	0.178	-0.088	0.0766	
KH80	0.173	-0.101	0.079	[13]
$\pi^- p$ 1s state	0.185	-0.104	0.081	[5]
Pearce et al.	0.151	-0.092	0.072	[18]
Schütz et al.	0.169	-0.085	0.074	[19]

TABLE II.  $\pi\pi$   $s$ -wave scattering lengths.

Source/Model	$a_0^0 [m_\pi^{-1}]$	$a_0^2 [m_\pi^{-1}]$	$(a_0^0 - a_0^2) [m_\pi^{-1}]$	Ref.
<i>Predictions from theory</i>				
Weinberg	0.16	-0.046	0.206	[26]
$\chi$ PT	0.20	-0.042	0.242	[16]
Meson exchange	0.31	-0.027	0.337	[15]
<i>Results from experiment</i>				
$K_{e4}$	$0.26 \pm 0.05$	$-0.028 \pm 0.012$	$0.288 \pm 0.051$	[27]
Chew-Low PSA	$0.24 \pm 0.03$	$-0.04 \pm 0.04$	$0.280 \pm 0.050$	[28]
Soft-Pion	$0.188 \pm 0.016$	$-0.037 \pm 0.006$	$0.225 \pm 0.017$	[29]
$\pi N \rightarrow \pi\pi N$	$0.205 \pm 0.025$	$-0.031 \pm 0.007$	$0.236 \pm 0.026$	[30]
<i>Results from inversion</i>				
Froggatt phase shifts	0.31	-0.059	0.369	
$\chi$ PT phase shifts	0.20	-0.043	0.243	
Meson ex. phase shifts	0.30	-0.025	0.325	



TABLE III.  $A_{\pi p}$   $1s$  level shift with respect to  $E_{1s}^C = 3234.9408$  eV and width. The strength of the imaginary  $W_{11}$  was adjusted to reproduce the experimental value.

Mass	Point Charge Coulomb		Gaussian Charge Coulomb		
	Shift [eV]	FWHM [eV]	Shift [eV]	FWHM [eV]	
$\mu_1 = \mu_2$	-7.29821	0.5250	-7.16746	0.5230	
$\mu_1 \neq \mu_2$	-7.13259	0.5187	-7.01055	0.5144	
	Shift = $-7.127 \pm 0.046$ [eV], $\Gamma_{1s}^{\pi^0 n} = 0.590$ [eV]				Sigg [5]
$\mu_1 \neq \mu_2$	-7.23259	0.9763	-7.12387	0.9763	$V_{11} + iW_{11}$
	Shift = $-7.127 \pm 0.028 \pm 0.036$ [eV], $\Gamma_{1s} = 0.97 \pm 0.10 \pm 0.05$ [eV]				Sigg [5]

TABLE IV.  $A_{\pi\pi}$  properties from inversion potentials

$E_{1s}$ [keV]	Shift [eV]	$\tau$ [ $10^{-15}$ s]	FWHM [eV]	Ref.
1.8638814	-5.809	1.97	0.3481	Froggatt [14]
1.8635114	-5.439	1.89	0.3627	Lohse [15]
1.8616174	-3.545	3.22	0.2128	$\chi_{PT}$ [16]
<i>Predictions from experimental analysis and other models</i>				
1.858		$2.9_{-2.1}^{+\infty}$		Afanasyev [6]
1.865	-7.0	3.2		Efimov [36]

TABLE V. Potential barrier positions.

Channel	$\pi N-\Delta$	$\pi\pi-\sigma$	$\pi\pi-\rho$	$K\pi-K_0^*$
Barrier radius [fm]	0.165	0.145	0.152	0.303

FIGURES

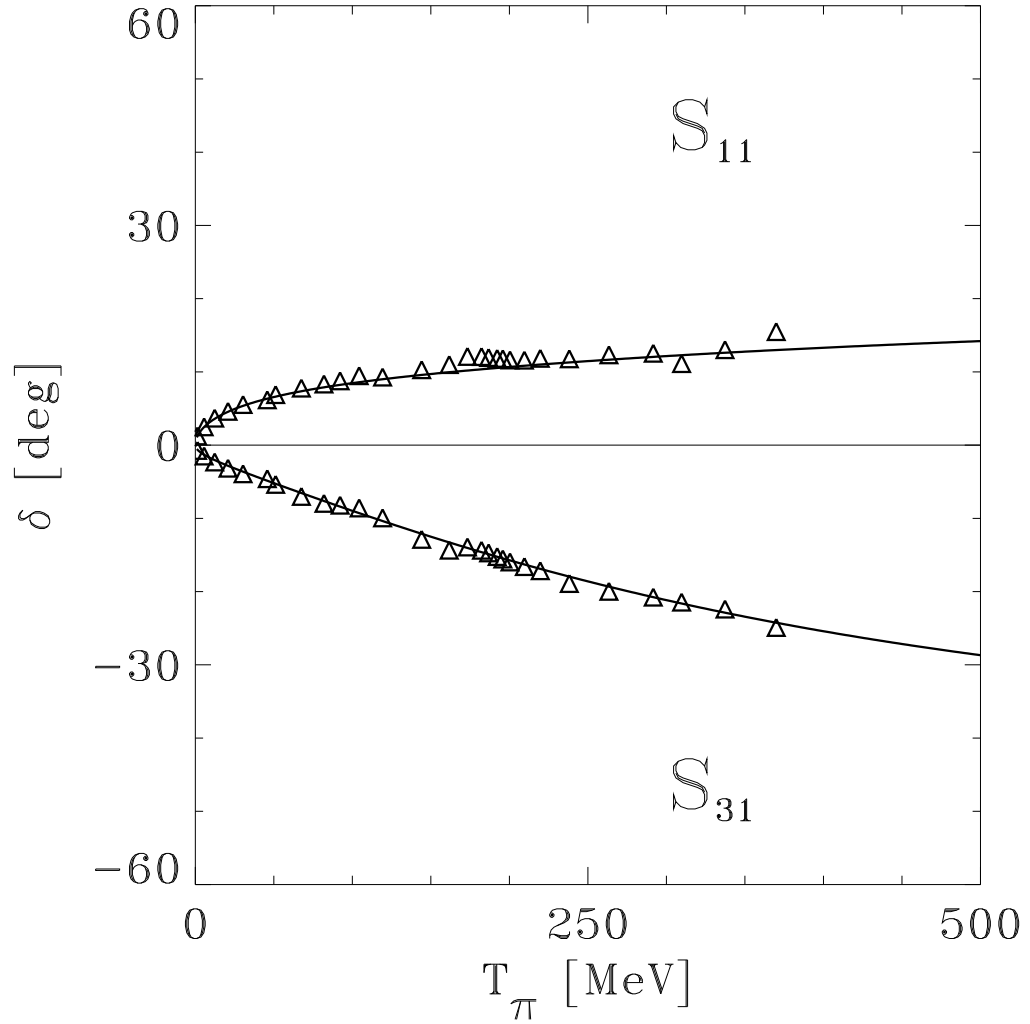


FIG. 1.  $\pi N$  SM95 [12] (coinciding with the solid line) and KH80 [13] (triangles) data and their reproduction by the inversion potentials (solid line) for the  $S_{11}$  and  $S_{31}$  channels.

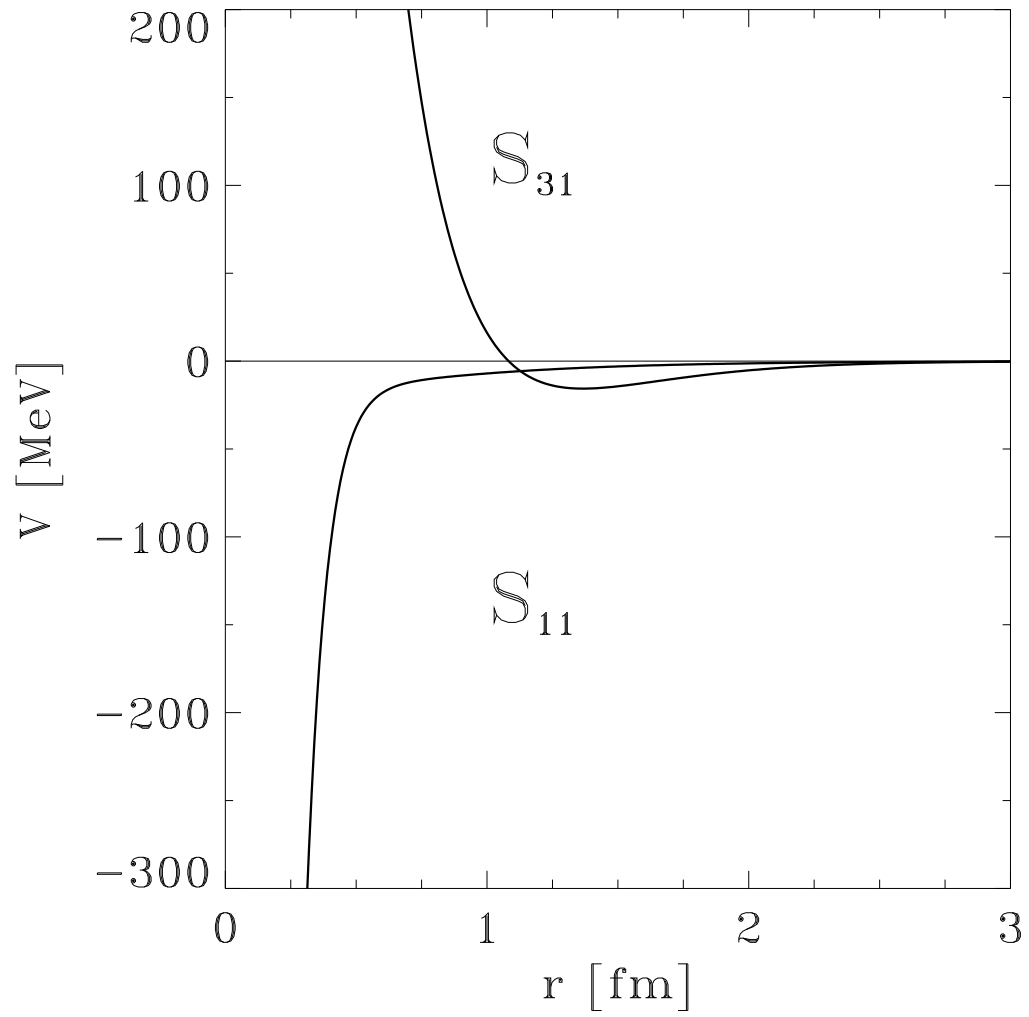


FIG. 2.  $S_{11}$  and  $S_{31}$  inversion potentials.

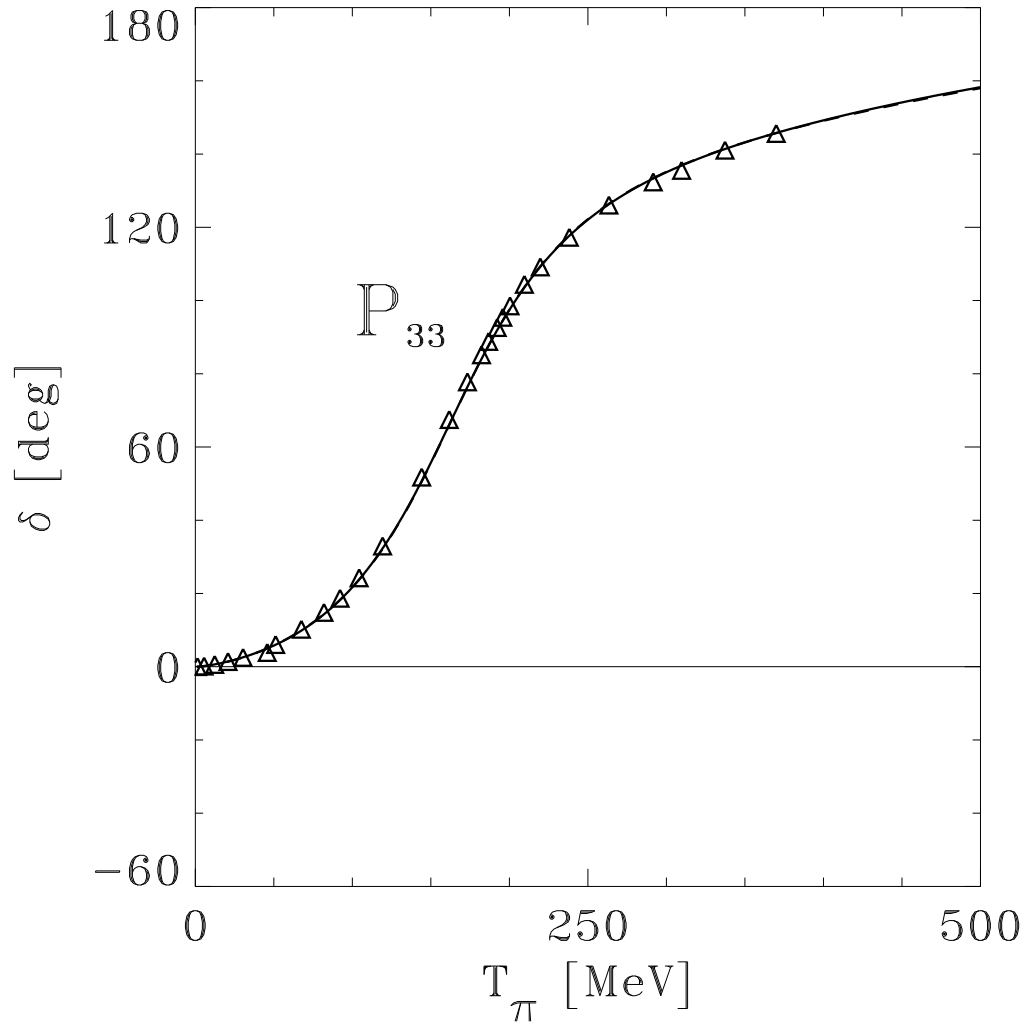


FIG. 3.  $\pi N$  SM95 [12] (coinciding with the solid line) and KH80 [13] (triangles) data and their reproduction by the inversion potential (solid line) for the  $P_{33}$  channel.

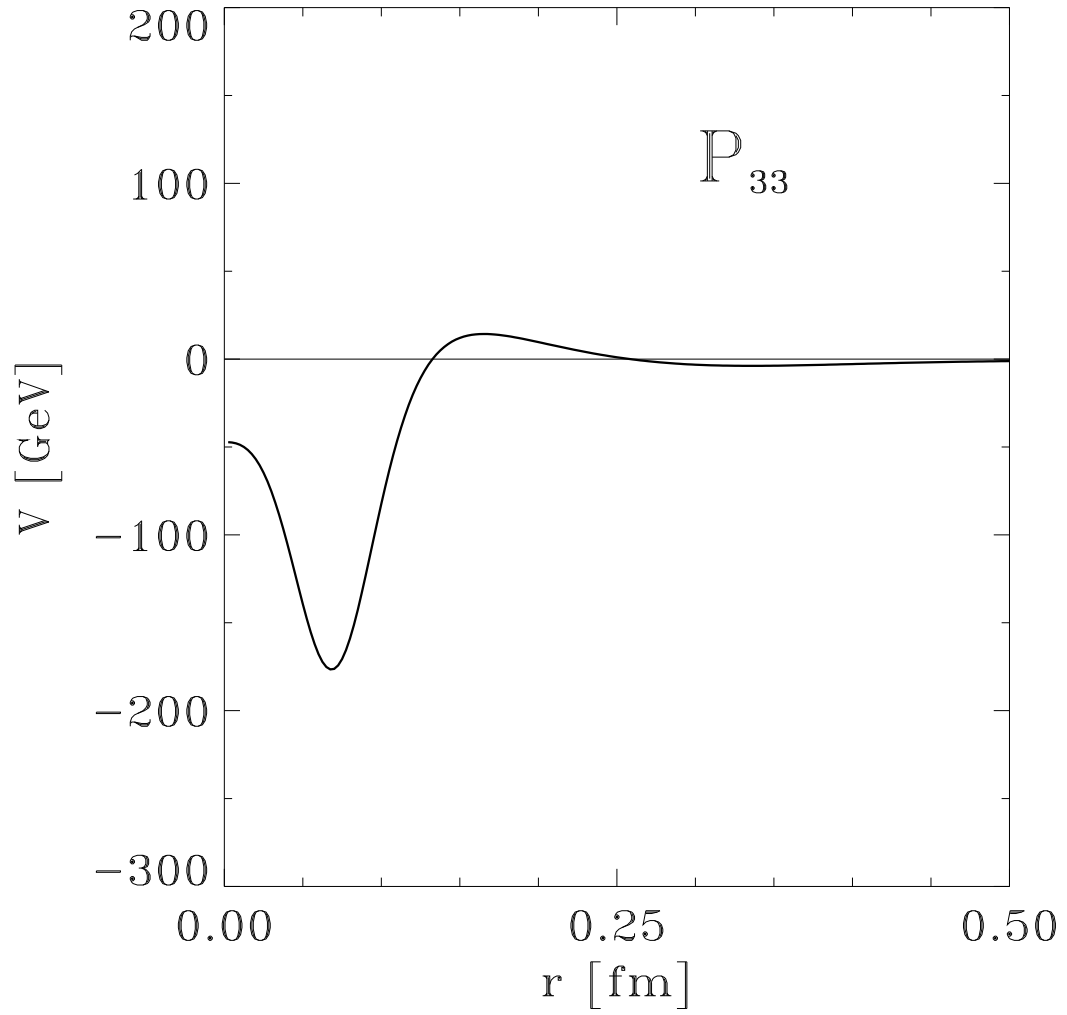


FIG. 4.  $P_{33}$  channel inversion potential.

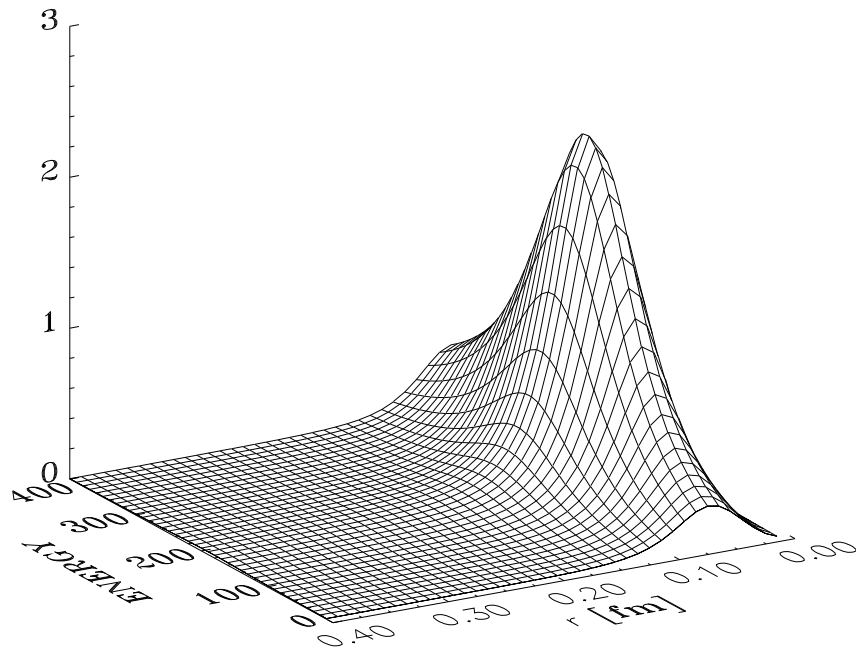


FIG. 5.  $\pi N P_{33}$  channel radial probability distribution as function of energy,  $T_{lab}$ .

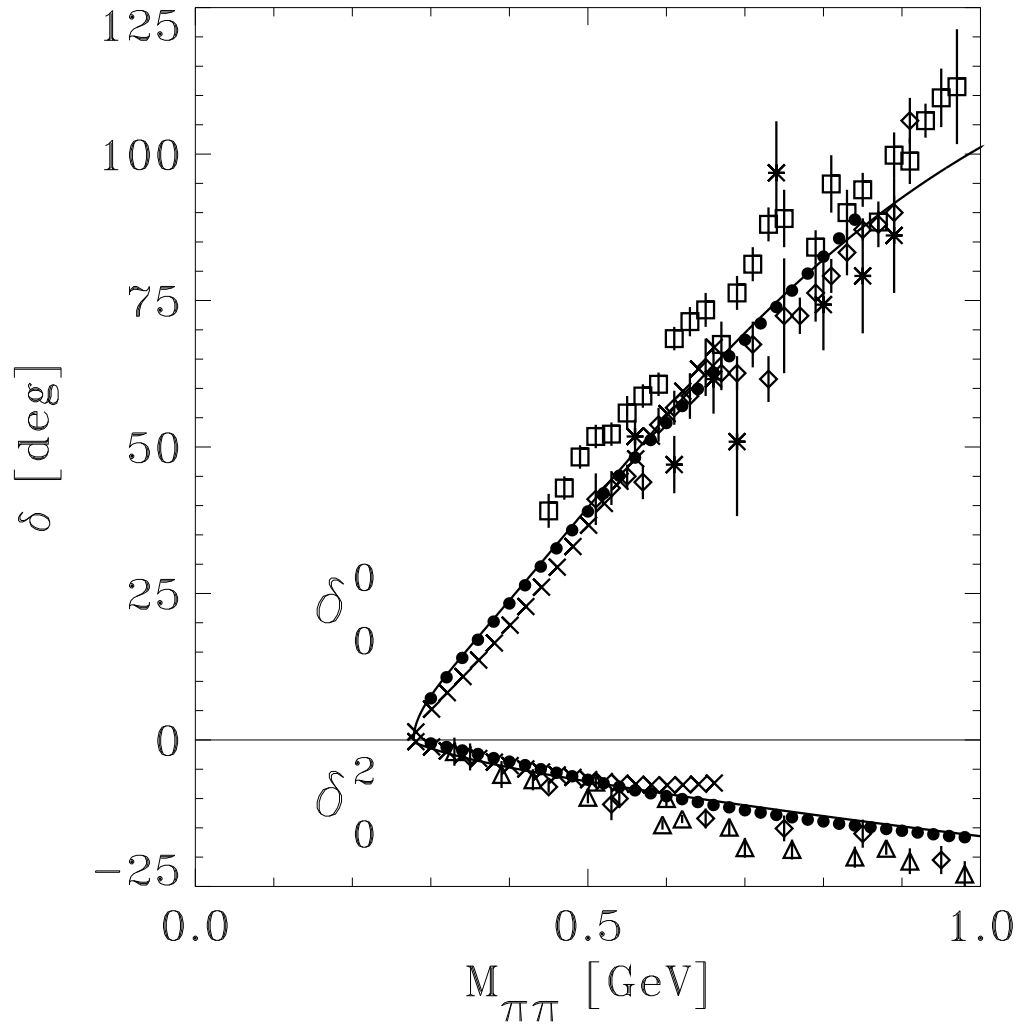


FIG. 6.  $\pi\pi$   $L = 0$ ,  $T = 0$  and 2 phase shifts. Froggatt data [14] and interpolation (dots and solid line),  $\chi$ PT [16] (crosses), Estabrooks et al. [22] (boxes), Grayer et al. [23] (diamonds), Männer [24] (triangles) and Baillon et al. [25] (asterixes).

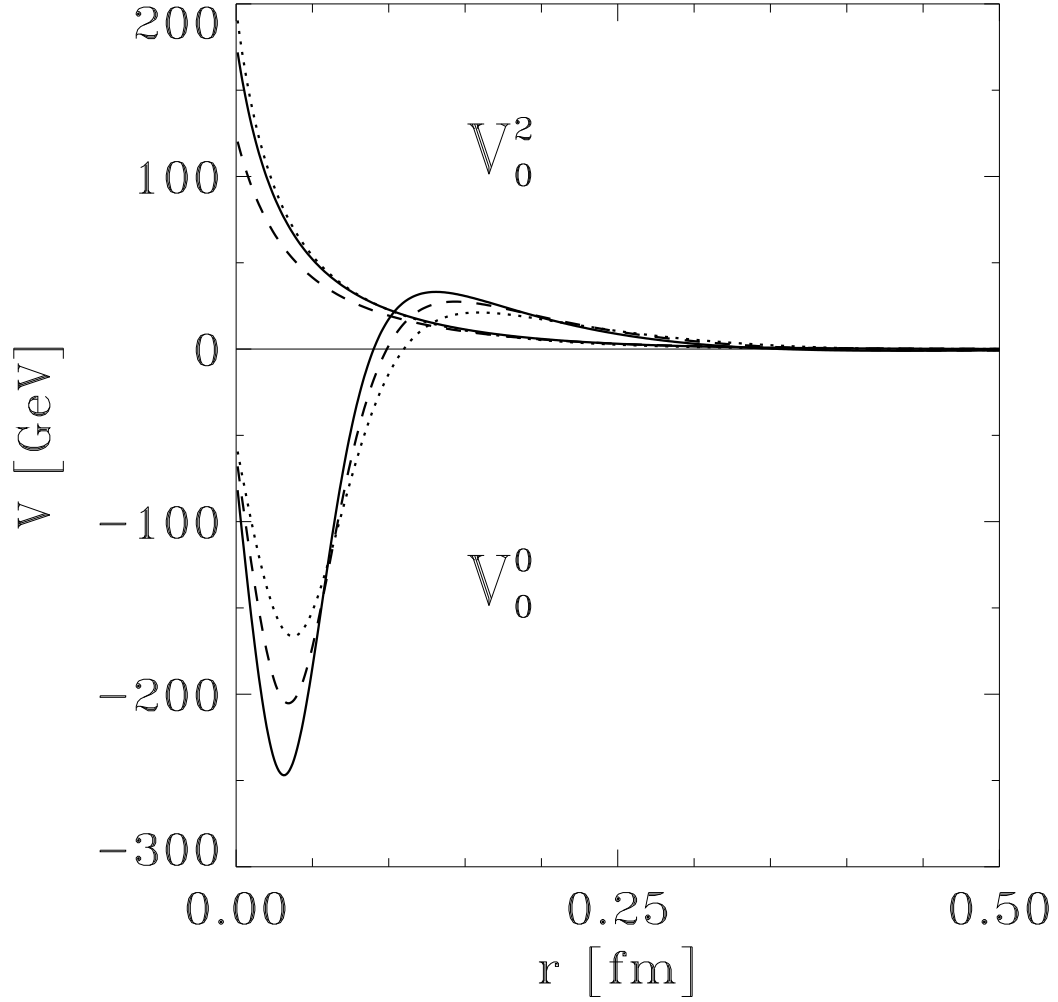


FIG. 7.  $\pi\pi$   $L = 0$ ,  $T = 0$  and 2 inversion potentials. Froggatt (solid line),  $\chi$ PT (dashed) and meson exchange [15] (dotted).



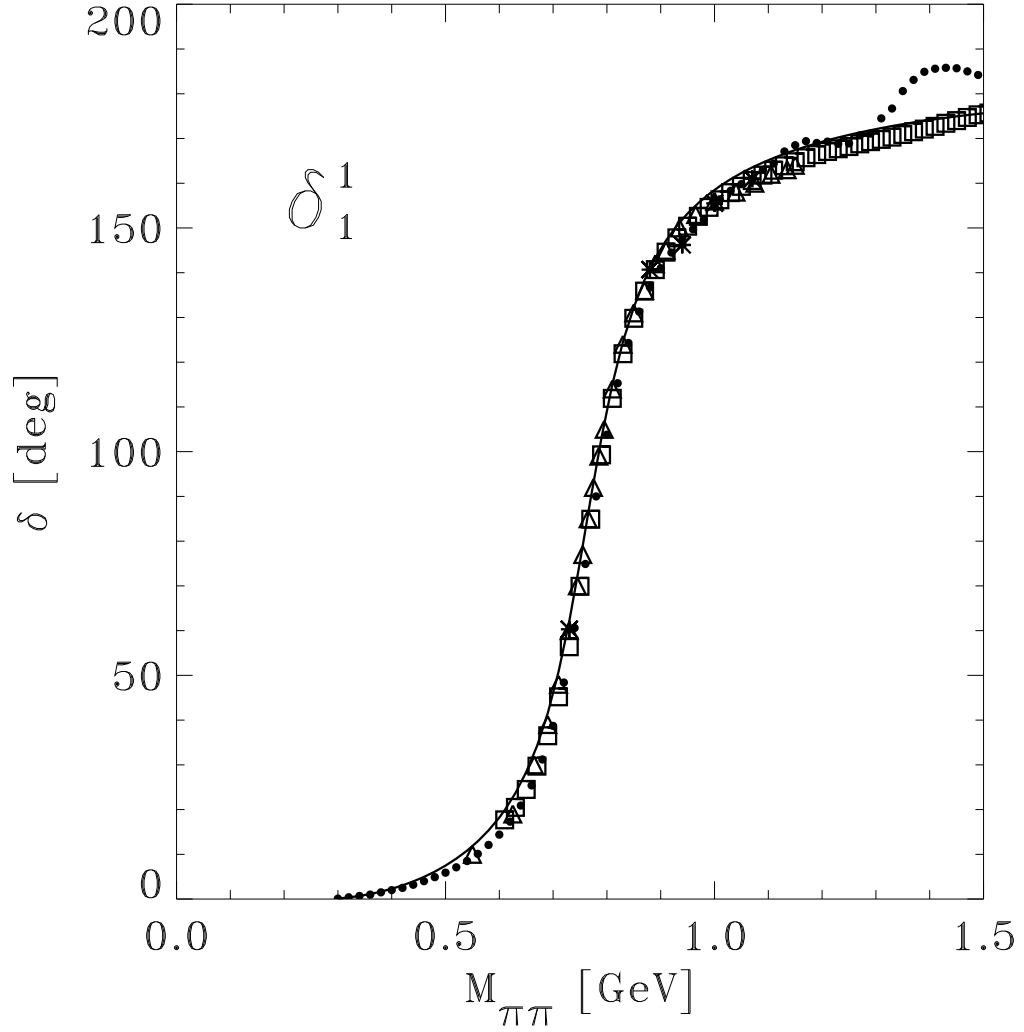


FIG. 8.  $\pi\pi$   $L = 1$ ,  $T = 1$  phase shifts. Data from Froggatt et al. [14] (dots), Ochs [31] (squares), Protopescu et al. [32] (triangles) and Deo et al. [33] (asterixes). Inversion result (solid line).

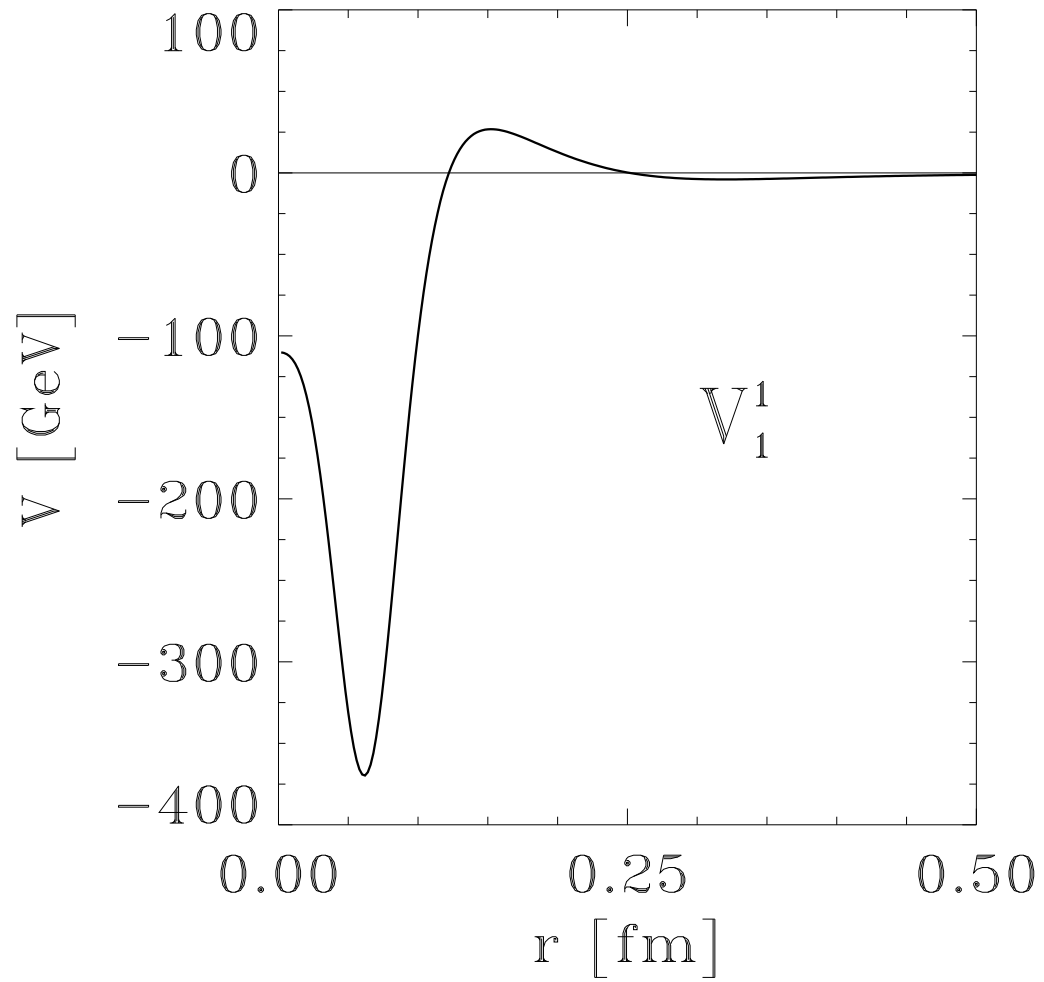


FIG. 9.  $\pi\pi$   $L = 1$ ,  $T = 1$  inversion potential.

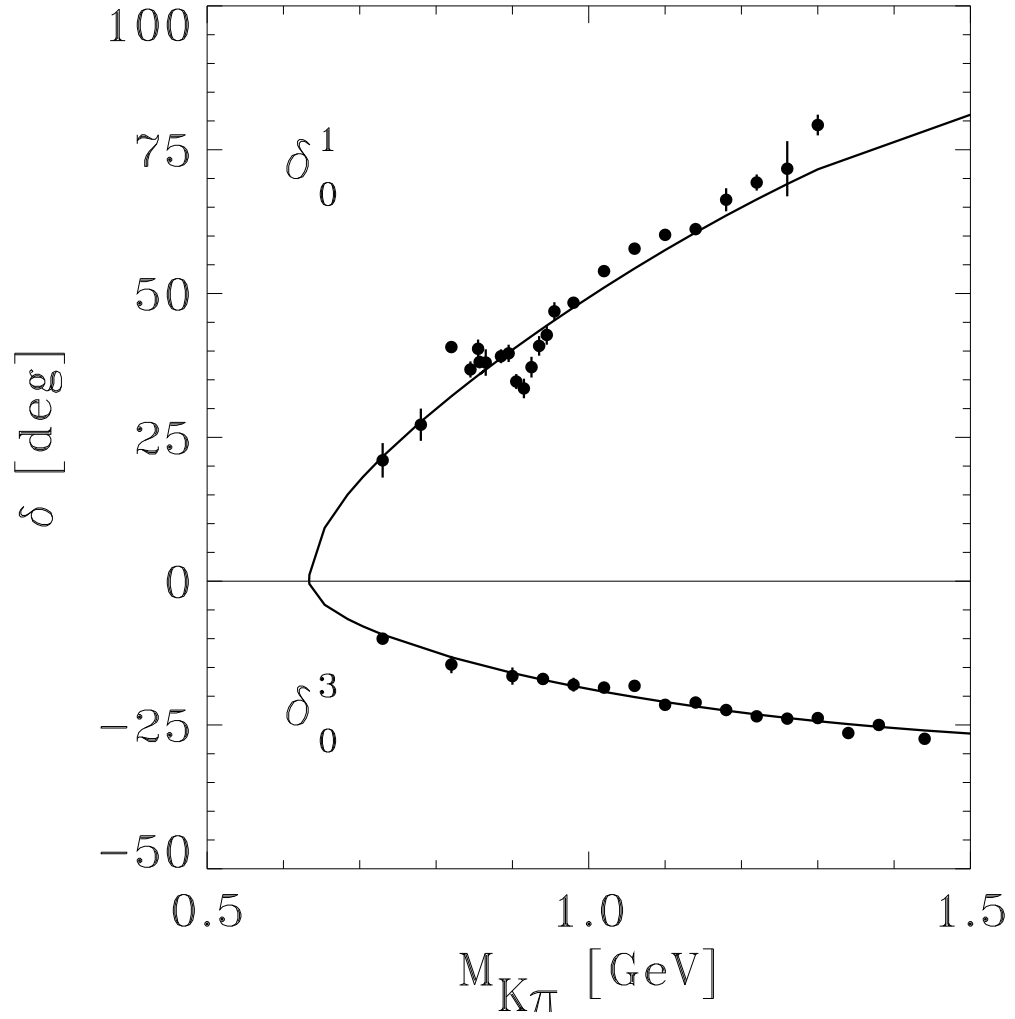


FIG. 10.  $K\pi$   $L = 0$ ,  $T = 1/2$  and  $3/2$  phase shifts. Data from Estabrooks et al. [17].

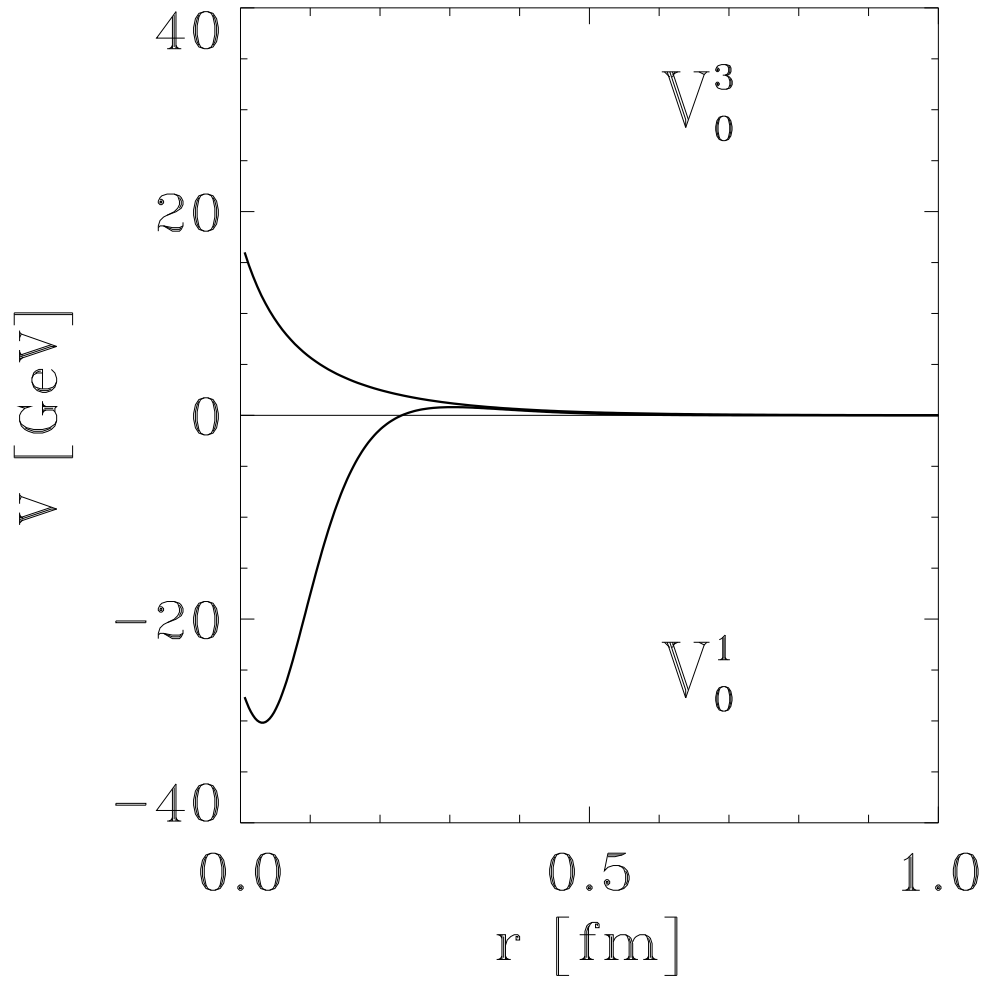


FIG. 11.  $K\pi$   $L = 0$ ,  $T = 1/2$  and  $3/2$  inversion potentials.

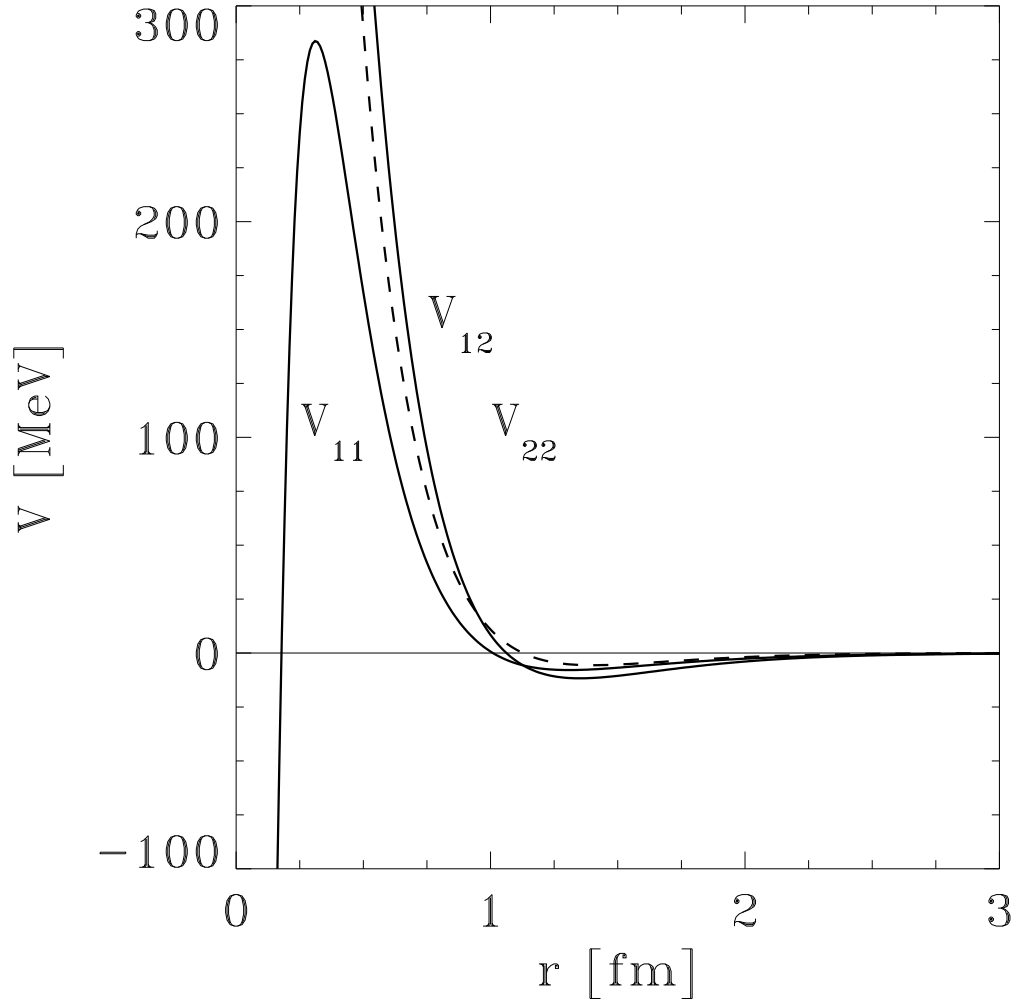


FIG. 12.  $\pi N$  hadronic potential matrix.

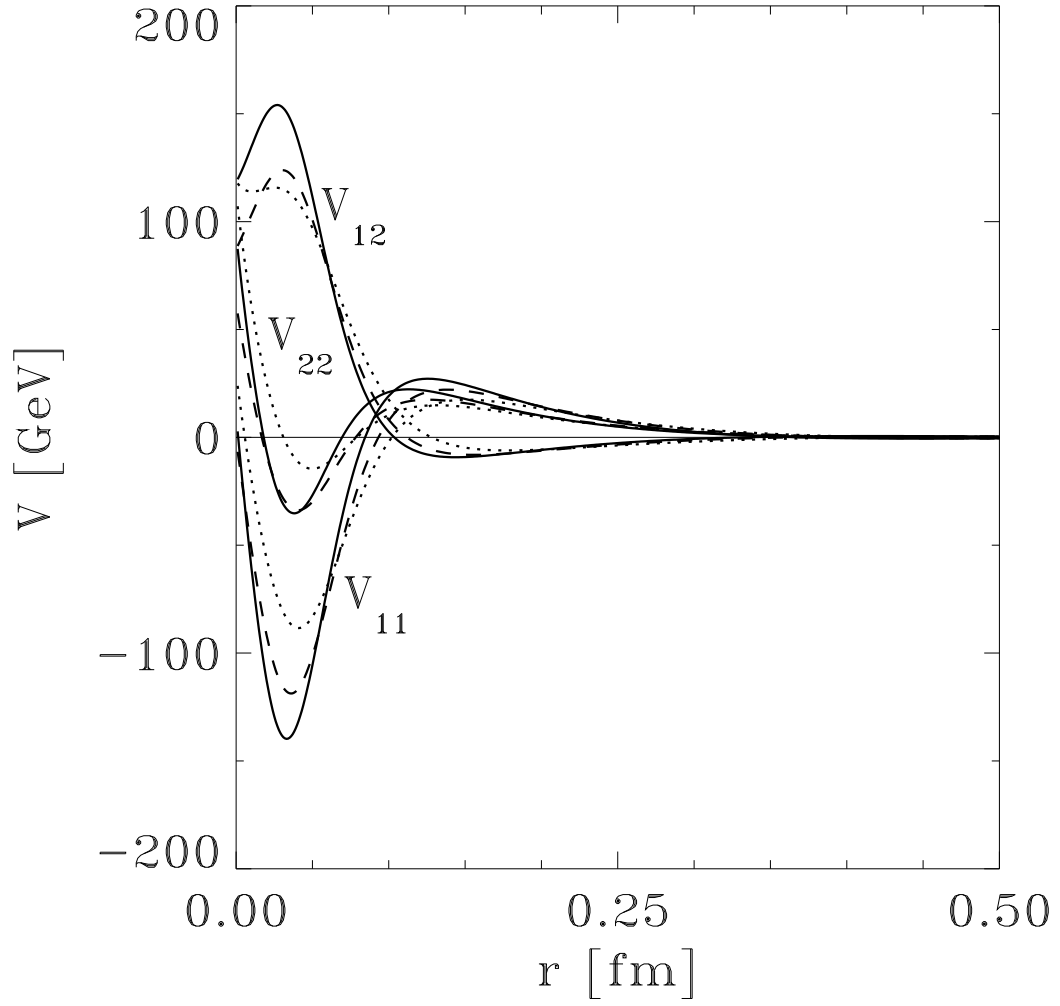


FIG. 13.  $\pi\pi$  hadronic potential matrix. Notation, see Fig. 7.

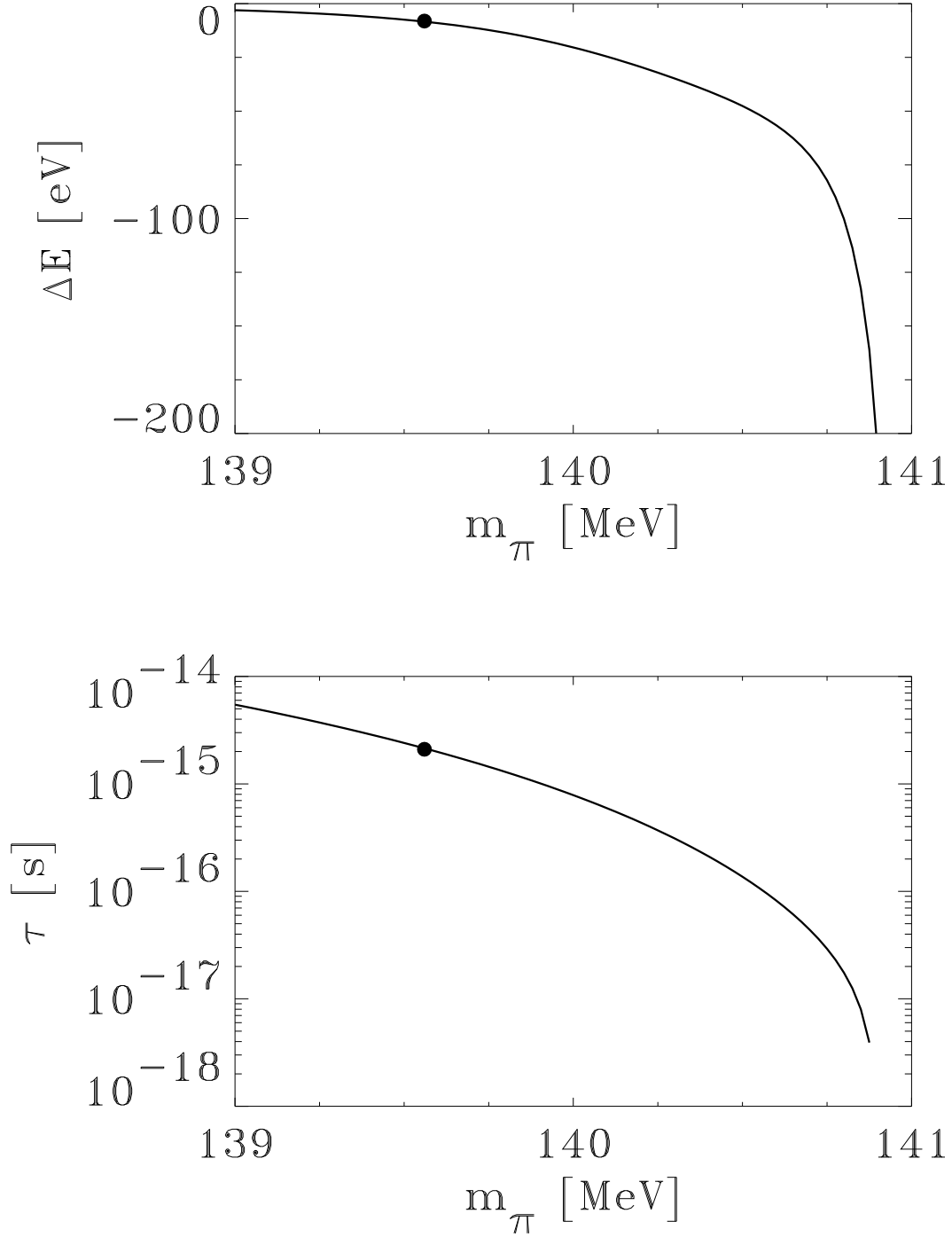


FIG. 14.  $A_{\pi\pi}$  shift (above) and width (below) as a function of the effective mass. The physical value  $m_{\pi^+} = 139.5676$  MeV is emphasized.

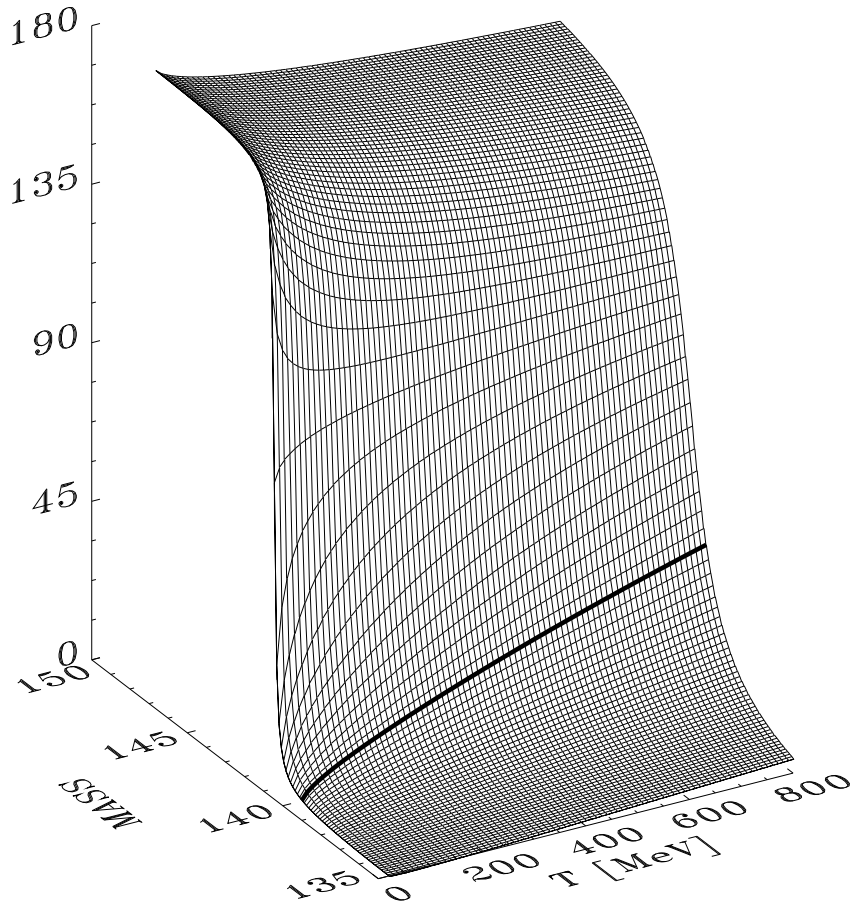


FIG. 15.  $\pi\pi$   $L = 0$ ,  $T = 0$  phase shift as a function of energy ( $T_{lab}$ ) and effective mass. The physical value  $m_{\pi^+} = 139.5676$  MeV is emphasized.



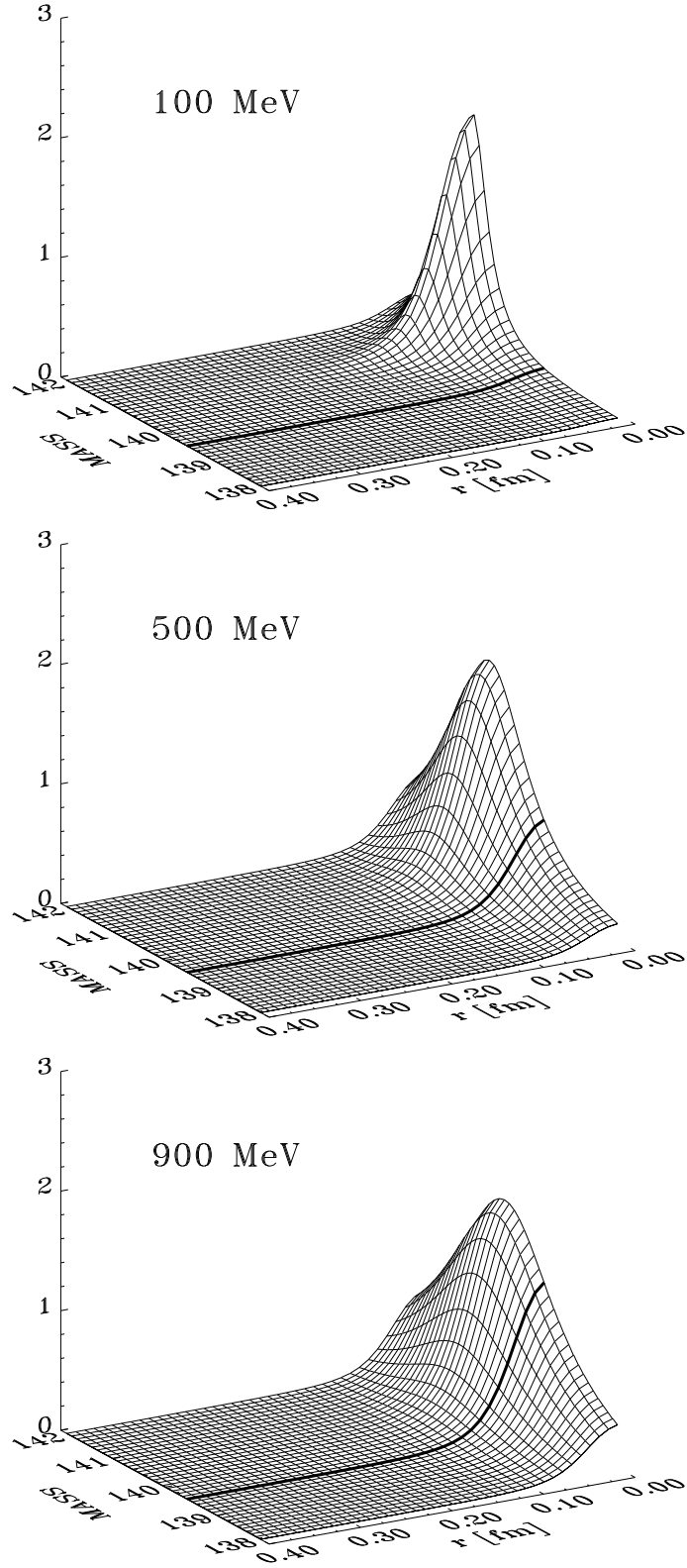


FIG. 16.  $\pi\pi$   $L = 0$ ,  $T = 0$  radial probability distribution as a function of effective mass given for three energies ( $T_{lab} = 100, 500$  and  $900$  MeV). The physical value  $m_{\pi^+} = 139.5676$  MeV is emphasized.

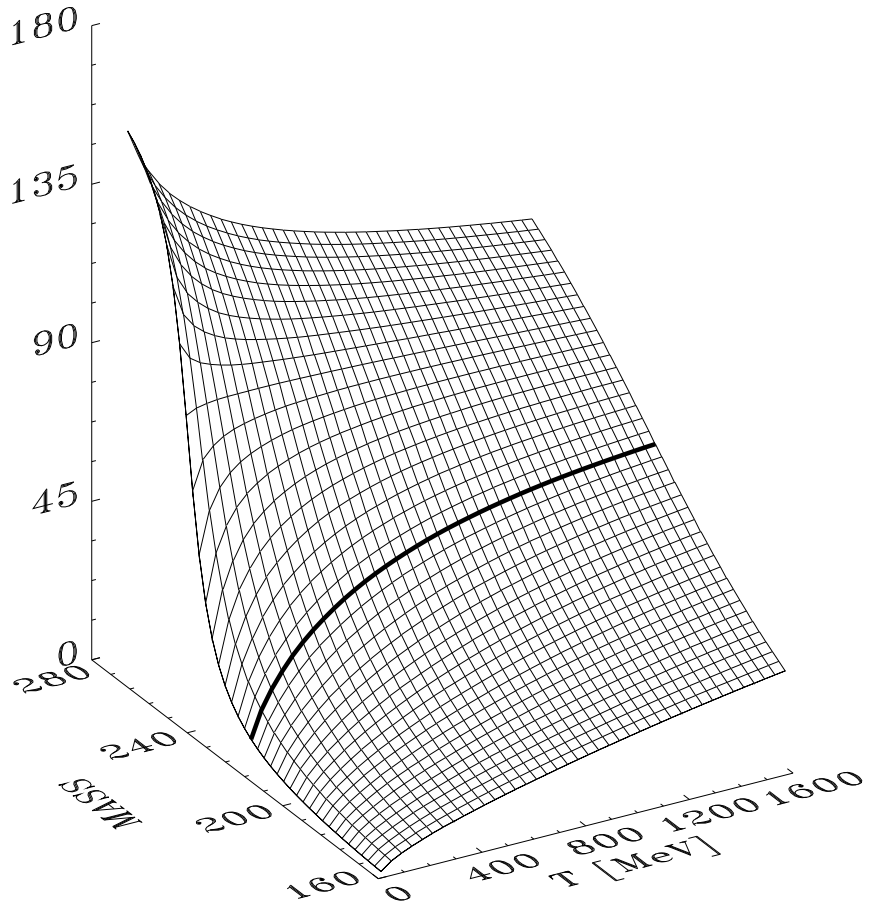


FIG. 17.  $K\pi$   $L = 0$ ,  $T = 1/2$  phase shift as a function of energy ( $T_{lab}$ ) and effective mass. The physical value  $2\mu_{K\pi} = 215.94$  MeV is emphasized.